Acta Cryst. (1995). B**51**, 709–721

Structures of $Ta_{22}W_4O_{67}$ and $Ta_{74}W_6O_{203}$. II. A Composite Modulated Structure Approach to the $(1-x)Ta_2O_5.xWO_3$, $0 \le x \le 0.267$, Solid Solution

BY A. DAVID RAE, SIEGBERT SCHMID, JOHN G. THOMPSON AND RAY L. WITHERS

Research School of Chemistry, Australian National University, Canberra, ACT 0200, *Australia*

AND NOBUO ISHIZAWA

Research Laboratory of Engineering Materials, Tokyo Institute of Technology, Nagatsuta, Midori-ku, Yokohama 226, *Japan*

(*Received* 31 *January* 1994; *accepted* 14 *March* 1995)

Abstract

The room-temperature commensurate single-crystal structures of $Ta_{22}W_4O_{67}$ [$M_r = 5788.19$, $a = 6.1485(5)$, $b = 47.6205(12)$, $c = 3.8559(3)$ Å, $\gamma = 90.04(1)°$, $C112/m$, $Z = 1$, $D_x = 8.513\ g\ cm^{-3}$] and $Ta_{74}W_6O_{203}$ [$M_r = 17741.06$, $a = 6.1664(5)$, $b = 29.2717(14)$, $c = 3.8731(2)$ Å, $Pbam$, $Z = 0.2$, $D_x = 8.428\ g\ cm^{-3}$] have each been refined using data sets collected with synchrotron radiation at three wavelengths near the Ta L_{III} absorption edge. The structures are parameterized and refined as composite modulated structures, composed of two interacting *Cmmm* parent substructures whose relative origins are separated by $\frac{1}{4}\mathbf{a} + \delta\mathbf{b}$. The parent substructures have the same a and c axial lengths, but the b axial lengths mismatch. Characteristic extinction conditions when the substructures are mutually incommensurable imply a superspace-group symmetry of $C'mmm(0,\alpha,0)s,-1,1$ with $\alpha \sim 1.62$. The refined atomic modulation functions describing the structural deviation of both substructures from their underlying parent substructures are shown to be remarkably similar for these two quite different compositions and are, therefore, most probably representative of the whole solid-solution range.

1. Introduction

The phase diagram of the Ta_2O_5–WO_3 system, and in particular the composition range from Ta_2O_5 to $Ta_{22}W_4O_{67}$, has been extensively studied by various authors (Roth, Waring & Parker, 1970; Roth & Stephenson, 1970; Williams, Tilley, Harburn & Williams, 1991; Schmid, Withers & Thompson, 1992). No two phase regions have ever been found below the solidus for any composition from Ta_2O_5 to $Ta_{22}W_4O_{67}$, implying the existence of a continuously variable, 'infinitely adaptive' solid solution over the composition range $(1-x)Ta_2O_5.xWO_3$, $0 \le x \le 0.267$. Despite this intensive investigation, the crystal chemistry underlying this continuous structural flexibility over such a wide composition range remains far from clear.

The diffraction pattern of any particular member of this solid solution is dominated by a set of strong Bragg reflections, $\mathbf{G}_M$, corresponding to a C-centred orthorhombic cell ($a_M \sim 6.20$, $b_M \sim 3.66$ and $c_M \sim 3.89$ Å) associated with the parent substructure of the metal atoms, see Fig. 1. Intensity equivalence and lack of systematic absences implies a parent substructure space group of *Cmmm* or a subgroup thereof. Numerous weaker satellite reflections also exist and these can be indexed as $\mathbf{G}_M \pm$ an integer times a primary modulation wavevector $\mathbf{q}_M$, whose relationship to composition was experimentally found to be given by $\mathbf{q}_M = (0.636-0.079x)\mathbf{b}_M^*$ (Schmid, Withers & Thompson, 1992), where x is continuous in the range $0 \le x \le 0.267$. In general, $\mathbf{q}_M$ is incommensurate.

Schmid, Withers & Thompson (1992) were the first to describe this system from a modulated structure perspective, describing the parent structure as anion-

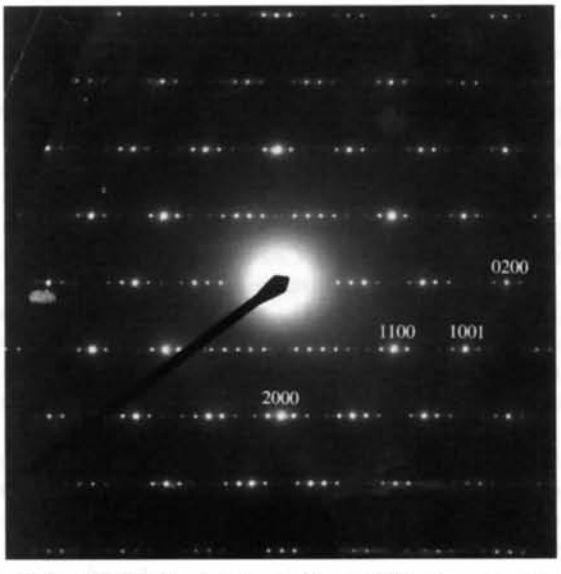

Fig. 1. A typical [001] selected-area electron-diffraction pattern for the $(1-x)Ta_2O_5.xWO_3$, $0 \le x \le 0.267$, solid solution field.

deficient α-UO_3-type with the modulation giving rise to the additional satellite reflections being attributed to ordering of metal atoms and anion vacancies, as well as associated atomic displacements, along the parent b direction. Characteristic extinction conditions associated with these satellites and the above choice of primary modulation wavevector implied a superspace-group symmetry of P: $Cmmm$: $s,-1,1$ (Schmid, Withers & Thompson, 1992).

During the course of the present work, however, it has become clear that the $(1-x)Ta_2O_5.xWO_3$, $0 \leq x \leq 0.267$, solid solution is better described as a composite modulated structure with large scale displacive modulations which are a consequence of the interaction of two, in general, mutually incommensurable parent substructures. The apparently continuous structural flexibility of this solid solution and the subtleties associated with the refinement of such structures can then be better understood. Our refinements of the superstructures $Ta_{22}W_4O_{67}$ and $Ta_{74}W_6O_{203}$ have used such a composite modulated structure approach and hence allowed the development of a general parameterization of the relationship between structure and composition for the range $0 \leq x \leq 0.267$.

2. Symmetry-allowed structural degrees of freedom

Composite modulated structures consist of two (or more) interpenetrating, often mutually incommensurable, parent substructures. The influence of these parent substructures upon each other leads to incommensurate modulation of the ideal fractional coordinates of both and to a resultant structure whose overall symmetry can be characterized by a $(3+d)$-dimensional superspace group (Janner & Janssen, 1980; van Smaalen, 1991; Yamamoto, 1992, 1993).

In the present case there is a strongly scattering metal oxide (or M) substructure and a weaker scattering oxygen (or O) substructure (see Fig. 2). The **a*** and **c*** reciprocal lattice vectors of both parent substructures are identical, whereas their colinear **b*** reciprocal lattice vectors are, in general, mutually incommensurable with $b_O^* = \alpha b_M^*$ and $\alpha \sim 1.6$. Characteristic extinction conditions (see below) require the parent substructures to each have at least $Cm11$ (but most probably $Cmmm$) space-group symmetry. The first parent substructure has a metal site M at $0,0,0$ and an oxygen site O_M at $0,0,\frac{1}{2}$, while the second parent substructure has an oxygen site O_O at $0,0,0$. Note that a lowering of these parent subgroup symmetries to a Cm-- subgroup of $Cmmm$ could be induced by shifting the parent O_M site relative to the metal in the b or c direction or by shifting the origin of the second substructure in the c direction. Such possibilities were investigated during refinement but were not found to be necessary.

In previous work, four-index notation (based upon the M substructure) was used to index any given reflection (Schmid, Withers & Thompson, 1992). Thus, observed reflections were indexed as $\mathbf{h} = h_M\mathbf{a}_M^* + k_M\mathbf{b}_M^* + l_M\mathbf{c}_M^* + m_M\mathbf{q}_M$, with $\mathbf{q}_M = (\alpha - 1)\mathbf{b}_M^*$. In terms of the M and O substructures defined above, this choice of primary modulation wavevector corresponds to $\mathbf{q}_M = (110)_O^* - (110)_M^* = \mathbf{b}_O^* - \mathbf{b}_M^*$. The observed extinction conditions, $F(hklm)_M = 0$ unless $h+k=2n$ and $F(0klm)_M = 0$ unless $k, m = 2n$, then implied an overall superspace-group symmetry of $Cmmm(0,\alpha\text{-}1,0)s$, $-1,1$ and the same superspace-group symmetry for each of the component substructures, with $\mathbf{q}_O = -\mathbf{q}_M = (110)_M^* - (110)_O^* = \mathbf{b}_M^* - \mathbf{b}_O^*$. Note that this is the standard setting for each subsystem superspace group (see Table 1 of de Wolff, Janssen & Janner, 1981).

In this paper, however, following a recently suggested convention as regards the choice of basis vectors for compositely modulated structures (Yamamoto, 1992, 1993), all reflections are indexed with respect to a basis set consisting of the fundamental reciprocal lattice vectors of the component substructures. Thus, all reflections are indexed with respect to the basis $M^* = \{\mathbf{a}^*, \mathbf{b}_M^*, \mathbf{c}^*, \mathbf{b}_O^*\}$ (see Fig. 1). With respect to this basis set, the observed extinction conditions are given by $F(HKLm) = 0$ unless $H+K+m=2n$ and $F(0KLm) = 0$ unless $K, m = 2n$. The former condition implies a non-standard centring in superspace of the form $\{\mathbf{1}|\frac{1}{2},\frac{1}{2},0,\frac{1}{2}\}$ (which we will hereafter label as C'), while the latter requires the presence of a glide plane $\{\mathbf{m}_x|0,0,0,\frac{1}{2}\}$. The presence of $(H,K,0,\text{odd})$ reflections (see Fig. 1), in conjunction with the general mmm diffraction symmetry, implies a mirror plane $\{\mathbf{m}_z|0000\}$ and an overall superspace-group symmetry of $C'mmm(0,\alpha,0)s,-1,1$. The M and O component sub-

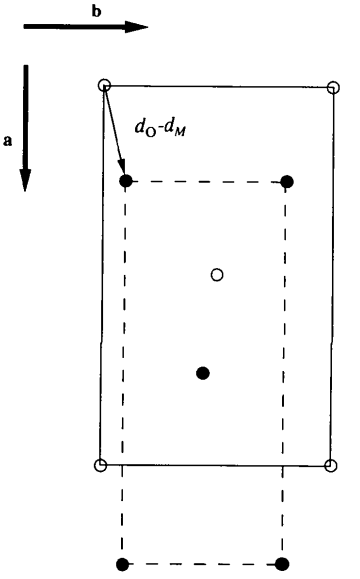

Fig. 2. The relative positions of the M and O substructures. Each parent substructure has $Cmmm$ symmetry.

system superspace groups (van Smaalen, 1991) can be derived from this overall superspace-group symmetry *via* the use of the appropriate permutation matrices [$W^M = P^M = (1)$ and $W^O = P^O = (2,4)$; Yamamoto (1993)] and are given by $C'mmm(0,\alpha,0)s,-1,1$ and $C'mmm(0,\alpha^{-1},0)s,-1,1$ respectively.

The glide plane $\{\mathbf{m}_x|0,0,0,\frac{1}{2}\}$ implies component substructure superspace-group operations $\{\mathbf{m}_x|0,0,0,\frac{1}{2}\}_M$ and $\{\mathbf{m}_x|0,\frac{1}{2},0,0\}_O$. Thus, the origin of the second (or O) parent substructure must be displaced by $(\mathbf{d}_O - \mathbf{d}_M) = \frac{1}{4}\mathbf{a} + \delta\mathbf{b}_O$ relative to the origin of the first (or M) substructure (see Fig. 2). Formally, the relative origin of both substructures along the b direction can be fixed *via* application of a superspace-group symmetry operation such as, for example, $\{\mathbf{m}_y|000,2\delta\}$. Application of this particular superspace-group symmetry operation implies $\mathbf{d}_M = 0$ and requires $\mathbf{d}_O - \mathbf{d}_M = \frac{1}{4}\mathbf{a} + \delta\mathbf{b}_O$ with respect to $\mathbf{d}_M$ as the origin. In conjunction with the other superspace-group symmetry operations, the exact form of the atomic modulation functions (AMF's; Pérez-Mato, Madariaga, Zúñiga & Garcia Arribas, 1987) describing the displacive, occupational and thermal parameter modulation of both parent substructures (see below) as a function of $\omega(\mathbf{t}_M) = \mathbf{q}_M.\mathbf{t}_M - \delta + \mathbf{a}_O^*.\mathbf{t}_M$ for the M substructure and $\omega(\mathbf{t}_O) = \mathbf{q}_O.(\mathbf{t}_O + [\mathbf{d}_O - \mathbf{d}_M]) + \mathbf{a}_M^*.\mathbf{t}_O$ for the O substructure can then be derived. Here, $\mathbf{t}_M$ and $\mathbf{t}_O$ represent Bravais lattice translations of the M and O substructures, while $\mathbf{q}_M = \mathbf{b}_O^*$ and $\mathbf{q}_O = \mathbf{b}_M^*$. The functional form of the AMF's (see below) is maintained for mutually commensurable substructures, but now different starting values for $(\mathbf{d}_O - \mathbf{d}_M)$ or δ can give rise to different space-group symmetries for the resultant three-dimensional supercell (see §3).

There are three atoms in the asymmetric unit (M and O_M for the M substructure and O_O for the O substructure; labelled $\mu = 1, 2$ and 3 below). The metal- ($\mu = 1$) and oxygen- ($\mu = 2$) atom positions within the parent M substructure are given by $\mathbf{t}_M + \mathbf{d}_M$ and $\frac{1}{2}\mathbf{c}_M + \mathbf{t}_M + \mathbf{d}_M$, respectively, while the O-atom ($\mu = 3$) position within the parent O substructure is given by $\mathbf{t}_O + \mathbf{d}_O$. Occupancy variation must necessarily occur for atoms of the M substructure, but was found to be unnecessary for the O substructure. The average metal-atom occupancy, $P_{\mu=1}$, is given by $(2-2x)/(2-x)\mathrm{Ta} + x/(2-x)\mathrm{W}$ [where x is the same x as in $(1-x)Ta_2O_5.xWO_3$], while the average O_M occupancy, $P_{\mu=2}$, is fixed by the stoichiometry. Thus, $P_{\mu=2}$ is given by $(5-2x)/(2-x) - \alpha$, where $\alpha = b_M/b_O$ is empirically given by $1.636-0.079x$.

The anisotropic thermal parameters U_{xz} and U_{yz} are identically zero for all three atoms because each occur on mirror planes perpendicular to c in the parent substructures. Since all atoms occur on special positions with *mmm* site symmetry in the parent substructures, odd-order modulation waves describe x displacements and U_{xy} variation, whereas even-order modulation waves describe y displacements, occupancy variation and variation in the thermal parameters U_{xx}, U_{yy}, U_{zz}. Values of U_{xy} will average zero.

The M substructure AMF's describing the displacive $[u_{\mu i}(\mathbf{l}|\mathbf{t}_M);\ i = x,y,z]$, occupational $[\Delta P_\mu(\mathbf{l}|\mathbf{t}_M)]$ and anisotropic thermal parameter deviations $[\Delta U_{ij}^\mu(\mathbf{l}|\mathbf{t}_M), i,j = x,y,z)$ from their average values as a function of $\omega(\mathbf{t}_M)$ are given by

$$u_{\mu x}(\mathbf{l}|\mathbf{t}_M) = \textstyle\sum_{2n+1} a_{\mu x}([2n+1]\mathbf{q}_M)\cos(2\pi[2n+1]\omega(\mathbf{t}_M)) \quad \mu = 1,2$$

$$u_{\mu y}(\mathbf{l}|\mathbf{t}_M) = \textstyle\sum_{2n} a_{\mu y}(2n\mathbf{q}_M)\sin(2\pi 2n\omega(\mathbf{t}_M)) \quad \mu = 1,2$$

$$\Delta U_{ii}^\mu(\mathbf{l}|\mathbf{t}_M) = \textstyle\sum_{2n} U_{ii}^\mu(2n\mathbf{q}_M)\cos(2\pi 2n\omega(\mathbf{t}_M)) \quad \mu = 1,2;\ i = x,y,z$$

$$\Delta U_{xy}^\mu(\mathbf{l}|\mathbf{t}_M) = \textstyle\sum_{2n+1} U_{xy}^\mu([2n+1]\mathbf{q}_M)\sin(2\pi[2n+1]\omega(\mathbf{t}_M)) \quad \mu = 1,2$$

$$\Delta P_\mu(\mathbf{l}|\mathbf{t}_M) = \textstyle\sum_{2n} P_\mu(2n\mathbf{q}_M)\cos(2\pi 2n\omega(\mathbf{t}_M)) \quad \mu = 1,2;$$

where $n = m_M$ is an integer which labels the harmonic order of the corresponding modulation wave with respect to the M substructure and $\omega(\mathbf{t}_M) = \mathbf{q}_M.\mathbf{t}_M - \delta + \mathbf{a}_O^*.\mathbf{t}_M$, modulo an integer. The M substructure AMF's are thus a periodic function of $\mathbf{q}_M.\mathbf{t}_M = \mathbf{b}_O^*.\mathbf{t}_M$, modulo an integer. Different M parent substructure unit cells are labelled by different values of $\mathbf{t}_M$ and give rise to necessarily different values of $\mathbf{q}_M.\mathbf{t}_M$ and hence $\omega(\mathbf{t}_M)$. Note, for example, that neighbouring parent substructure unit cells along $\mathbf{b}_M$ are separated by $\mathbf{q}_M.\mathbf{b}_M = \mathbf{b}_O^*.\mathbf{b}_M = \alpha$ in $\omega(\mathbf{t}_M)$ and hence are not neighbouring as far as $\omega(\mathbf{t}_M)$ is concerned.

The corresponding O substructure AMF's are given by

$$u_{3x}(\mathbf{l}|\mathbf{t}_O) = \textstyle\sum_{2n+1} a_{3x}([2n+1]\mathbf{q}_O)\cos(2\pi[2n+1]\omega(\mathbf{t}_O))$$

$$u_{3y}(\mathbf{l}|\mathbf{t}_O) = \textstyle\sum_{2n} a_{3y}(2n\mathbf{q}_O)\sin(2\pi 2n\omega(\mathbf{t}_O))$$

$$\Delta U_{ii}^3(\mathbf{l}|\mathbf{t}_O) = \textstyle\sum_{2n} U_{ii}^3(2n\mathbf{q}_O)\cos(2\pi 2n\omega(\mathbf{t}_O)) \quad i = x,y,z;$$

$$\Delta U_{xy}^3(\mathbf{l}|\mathbf{t}_O) = \textstyle\sum_{2n+1} U_{xy}^3([2n+1]\mathbf{q}_O)\sin(2\pi[2n+1]\omega(\mathbf{t}_O)),$$

where $n = m_O$ is an integer which labels the harmonic order of the corresponding modulation wave with respect to the O substructure and $\omega(\mathbf{t}_O) = \mathbf{q}_O.(\mathbf{t}_O + [\mathbf{d}_O - \mathbf{d}_M]) + \mathbf{a}_M^*.\mathbf{t}_O$, modulo an integer. The parameter $\omega(\mathbf{t}_O)$ is a label for the different values of $\mathbf{q}_O.\mathbf{t}_O = \mathbf{b}_M^*.\mathbf{t}_O$.

Note that the superspace-symmetry operation $\{\mathbf{m}_z|0000\}$ forbids displacive modulation along c for either substructure. The possibility of lowering the overall superspace-group symmetry to a $C'm$--$(0,\alpha,0)s$-- subgroup of $C'mmm(0,\alpha,0)s,-1,1$ was care-

fully considered, but no evidence could be found justifying the lowering of the latter symmetry.

Structure refinement consists of determining the parent substructure positions, occupancies and thermal parameters as well as the above modulation wave amplitudes (both magnitude and sign). The magnitude of such modulation wave amplitudes almost invariably decay rapidly with increasing harmonic order (*i.e.* with increasing n), so that only a limited number ever need to be determined.

3. Implications of commensurability

As described in Part I (Schmid *et al.*, 1995), the diffraction data collected for $Ta_{22}W_4O_{67}$ showed $112/m$ diffraction symmetry rather than the *mmm* diffraction symmetry that the above superspace group requires when the two substructures are mutually incommensurable. It is therefore important to consider the implications of commensurability. $Ta_{22}W_4O_{67}$ crystallizes in an apparently C-centred superstructure with $b_M/b_O = 21/13$, while $Ta_{74}W_6O_{203}$ crystallizes in an apparently primitive superstructure with $b_M/b_O = 13/8$. The possible three-dimensional space-group symmetries appropriate to $Ta_{22}W_4O_{67}$ and $Ta_{74}W_6O_{203}$ can then be obtained directly from the superspace-group symmetry.

Each element $(\mathbf{R}, \varepsilon|\tau_1, \tau_2, \tau_3, \tau_4)$ of the superspace group defines a three-dimensional space-group symmetry operation of the supercell if $\mathbf{a}_4^*.(\tau_1\mathbf{a}_1 + \tau_2\mathbf{a}_2 + \tau_3\mathbf{a}_3) = \tau_4$, modulo 1 (Yamamoto & Nakazawa, 1982; Wiegers *et al.*, 1990). In our particular case $\mathbf{a}_4^* = \mathbf{b}_O^*$. Hence, for example, the superspace-group centring translation $(\mathbf{1}|\frac{1}{2}, \frac{13}{2}, 0, \frac{1}{2})$ becomes the C-centring Bravais lattice translation of the $b = 13b_M$ supercell of $Ta_{22}W_4O_{67}$, while the superspace-group glide plane $(\mathbf{m}_x|0, 4, 0, \frac{1}{2})$ becomes a b-glide operation of the $b = 8b_M$ supercell of $Ta_{74}W_6O_{203}$. Other supercell symmetry operations can be obtained similarly. When $\varepsilon = -1$, the possibility of a three-dimensional symmetry operation depends on the relative positions of the two substructures, *i.e.* upon $\mathbf{d}_O - \mathbf{d}_M = \frac{1}{4}\mathbf{a} + \delta\mathbf{b}_O$, or, equivalently, on the value of δ in the symmetry operator $(\mathbf{m}_y|0, 0, 0, 2\delta)$.

For $Ta_{22}W_4O_{67}$, the possible resultant supercell space-group symmetries are

$C2mm$ (for $\delta = 2N/52$, integer N)
$C112/m$ [for $\delta = (2N + 1)/52$]
and $C11m$ otherwise.

For $Ta_{74}W_6O_{203}$, the possible resultant supercell space-group symmetries are

$Pbmm$ (for $\delta = 2N/32$, integer N)
$Pbam$ [for $\delta = (2N + 1)/32$]
and $Pb2_1m$ otherwise.

Even though the measured monoclinic angle barely deviated from 90° [$\gamma = 90.04(1)°$, see Part I], the data collected from the crystal of $Ta_{22}W_4O_{67}$ used for the present study clearly showed $C112/m$ diffraction symmetry, thus implying 'lock-in' of δ to $(2N + 1)/52$, with N an integer. The *mmm* diffraction symmetry of $Ta_{74}W_6O_{203}$, on the other hand, is compatible with any value of δ. For both crystal chemical and refinement reasons (see models 1 and *Pbmm* of Table 5 for example), however, the structure is best refined in space group *Pbam*.

For $Ta_{22}W_4O_{67}$, note that the smallest shift in δ required to change from space group $C112/m$ to $C2mm$ is $\frac{29}{4}\mathbf{b}_O - \frac{9}{2}\mathbf{b}_M = \frac{1}{52}\mathbf{b}_O = \frac{1}{84}\mathbf{b}_M \sim 0.044$ Å and corresponds to switching from a centre of inversion on $M1$ to $M4$ being on an exact mirror plane perpendicular to **b** (see Fig. 3). For $Ta_{74}W_6O_{203}$, the smallest shift of $\frac{5}{4}\mathbf{b}_M - 2\mathbf{b}_O = \frac{1}{32}\mathbf{b}_O = \frac{1}{52}\mathbf{b}_M \sim 0.070$ Å required to change from space-group *Pbam* to *Pbmm* corresponds to switching from an oxygen being on a centre of inversion to a metal being on a centre of inversion. This places $M4$ on an exact mirror plane perpendicular to **b** (see Fig. 4).

4. Refinement strategy

The structural parameterization and refinement of truly incommensurately modulated structures in terms of modulation wave parameters [the $a_{\mu i}(n\mathbf{q}_M)$'s *etc.* given above] is unavoidable. Such structural parameterization is still of great advantage even for commensurately modulated structures, where individual atom-based parameters could be used instead. In the case of modulated solid solutions, for example, it enables a quantitative comparison of structure as a function of composition to be made. Furthermore, modulation wave magnitudes almost invariably decay rapidly with increasing harmonic order (*i.e.* with increasing n). Hence, the intensities of observed superstructure reflections almost invariably also decay rapidly with increasing harmonic order (assuming the appropriate primary modulation wavevector can be correctly identified; Pérez-Mato, Madariaga, Zúñiga & Garcia Arribas, 1987).

This allows a hierarchical approach to structure refinement in which the higher-order (*i.e.* large n) modulation wave amplitudes are initially constrained to be zero, while the larger magnitude modulation wave amplitudes associated with low values of n are first determined. The structural degrees of freedom associated with the higher-order values of n are released for refinement only after the lower-order modulation wave amplitudes are successfully determined. Such a hierarchical approach to superstructure refinement helps avoid pitfalls [such as falling into non-self-correcting false minima (Rae, Thompson, Withers & Willis, 1991) or of excessively noisy AMF's (Withers, Schmid & Thompson, 1993)] associated with a simple atom-based approach where all structural degrees of freedom are simultaneously released.

In the case of composite structures, such a refinement strategy is complicated by the fact that both substructures contribute to the observed reflections, usually at different harmonic orders m_M and m_O. In the present case, however, the large difference in scale between the contributions from the strongly scattering M and the weaker scattering O substructures means that the M substructure dominates the phase determination of all reflections. It is therefore appropriate to segment and monitor reflection data in terms of the harmonic order of the reflections with respect to the M rather than the O substructure. Only when the large magnitude, low-harmonic order (*i.e.* low m_M) modulation wave amplitudes have been successfully determined *via* comparative refinement were the remaining structural degrees of freedom associated with the M and O substructures released for refinement.

While the supercell structure factors were always calculated exactly in terms of individual atom-based parameters, the least-squares refinement procedure was based upon the above modulation wave parameterization, *i.e.* the individual atom-based parameters within the two

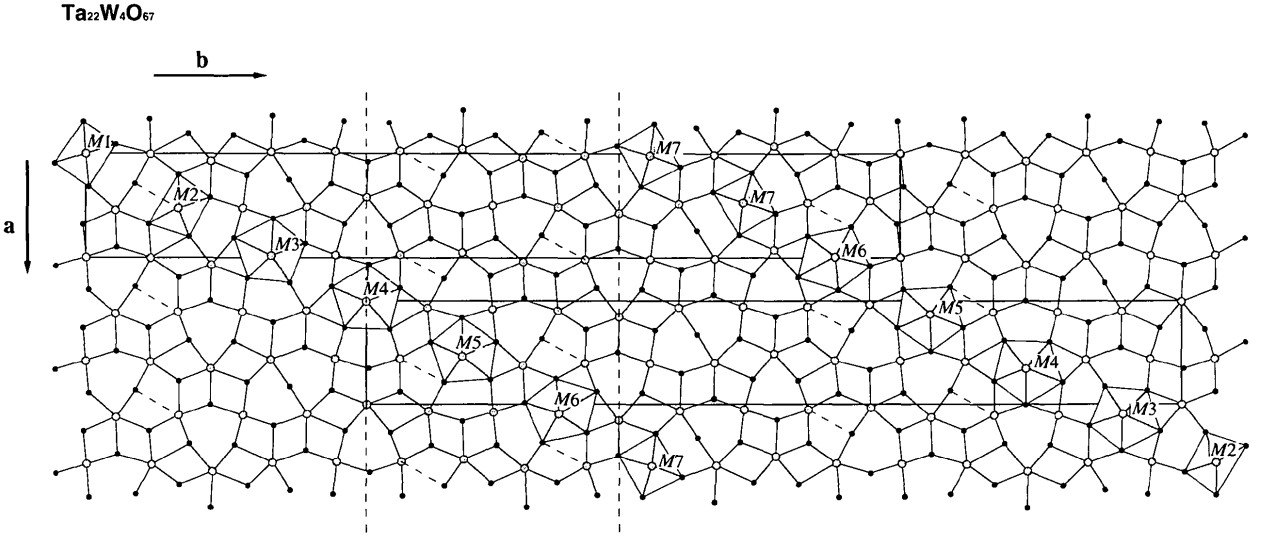

Fig. 3. Projection down **c*** of the $C112/m$, $Z = 1$, structure of $Ta_{22}W_4O_{67}$. *M*4 atoms lie approximately on pseudo-mirror planes used to partially disorder the structure, shown by dashed lines. *M*5 atoms also lie approximately on pseudo-mirror planes. Two unit cells are shown. The second is for a standard setting of *C*2*mm*.

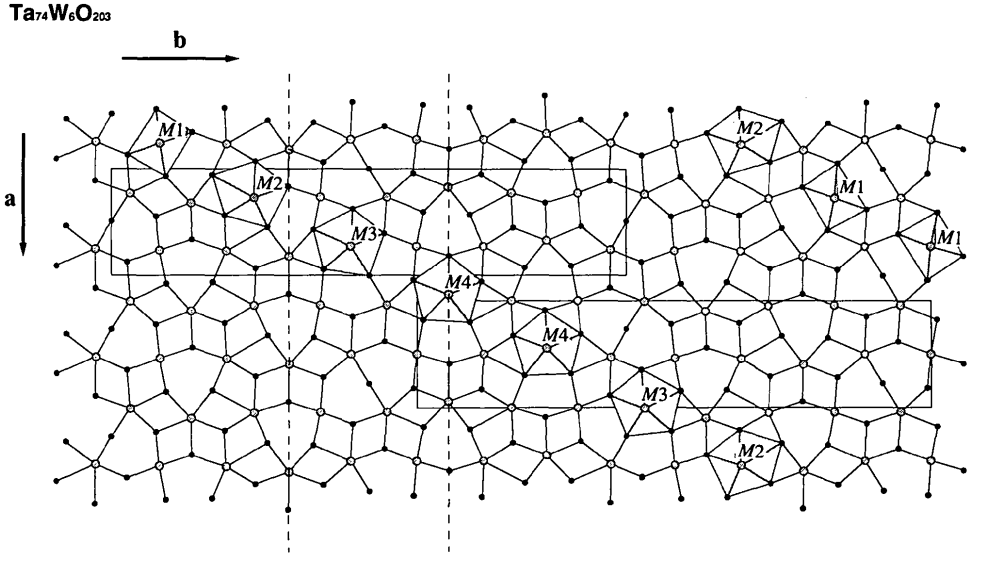

Fig. 4. Projection down **c*** of the *Pbam*, $Z = 0.2$, structure of $Ta_{74}W_6O_{203}$. *M*4 atoms lie approximately on pseudo-mirror planes used to partially disorder the structure. Two unit cells are shown, the second is for a standard setting of *Pbmm*.

supercells were expressed as functions of the above modulation wave amplitudes so that least-squares minimization could be carried out with respect to either modulation wave amplitudes or with respect to individual atom-based parameters.

5. Refinement details

$Ta_{22}W_4O_{67}$ crystallizes in an apparently C-centred superstructure with $b_M/b_O = \frac{21}{13}$, while $Ta_{74}W_6O_{203}$ crystallizes in an apparently primitive superstructure with $b_M/b_O = \frac{13}{8}$. [Note the closeness of these ratios to the so-called Golden Mean $\tau = (1 + 5^{1/2})/2$]. Hence, $\mathbf{q}_M = \mathbf{a}^* + \frac{21}{13}\mathbf{b}_M^*$ and $\mathbf{q}_O = \mathbf{a}^* + \frac{13}{21}\mathbf{b}_O^*$ for $Ta_{22}W_4O_{67}$, while $\mathbf{q}_M = \mathbf{a}^* + \frac{13}{8}\mathbf{b}_M^*$ and $\mathbf{q}_O = \mathbf{a}^* + \frac{8}{13}\mathbf{b}_O^*$ for $Ta_{74}W_6O_{203}$. Note that $13\mathbf{q}_M = \mathbf{G}_M$ for $Ta_{22}W_4O_{67}$, while $16\mathbf{q}_M = \mathbf{G}_M$ for $Ta_{74}W_6O_{203}$. Thus, satellites of the order m_M and $13 \pm m_M$ coincide for $Ta_{22}W_4O_{67}$, whereas satellites of the order m_M and $16 \pm m_M$ coincide for $Ta_{74}W_6O_{203}$. To help analyse the structure refinements, each reflection was assigned an index corresponding to the minimum magnitude of m_M for that reflection, 0–6 for $Ta_{22}W_4O_{67}$ and 0–8 for $Ta_{74}W_6O_{203}$. Refinement statistics were monitored according to these indices (see Tables 2 and 5). As expected, the intensity of observed reflections did indeed fall off as this index increased, but significant numbers of reflections were nonetheless observed in all index classes for both structures. It is worth pointing out here that the final refined amplitudes of the $m_M = 1, 2$ and 3 displacive modulation waves (see Table 1) were found to be sufficiently large to cause observable intensity in all index classes of satellite reflections for both $Ta_{22}W_4O_{67}$ and $Ta_{74}W_6O_{203}$.

The program *RAELS*89 (Rae, 1989) was used to minimize $\sum_{\mathbf{h}} w_{\mathbf{h}}||F_{obs}(\mathbf{h})| - |F_{calc}(\mathbf{h})||^2$. For $Ta_{22}W_4O_{67}$, an additional uncorrelated 4% error in $|F_{obs}(\mathbf{h})|$ was included together with the counting statistic estimate in the evaluation of weights for least squares. A value of 2% was used for $Ta_{74}W_6O_{203}$. The effect of this was to more equally distribute goodness-of-fit values over the data classes and, in the case of the $C112/m$ $Ta_{22}W_4O_{67}$ structure refinement, accentuate reflections that best determine twin and disorder parameters.

While the data collected from the crystal of $Ta_{22}W_4O_{67}$ had $112/m$ diffraction symmetry, it was still possible that the crystal was twinned perpendicular to x – particularly as the crystal used for the present study was a fragment of a larger crystal which showed a 1:1 twin ratio within error when data were collected with Mo $K\alpha$ radiation. If $Ta_{22}W_4O_{67}$ has a twin ratio $(1 - \alpha) : \alpha$ then the intensities of reflections $\mathbf{h} = (HKLm)$ are given by

$$Y(\mathbf{h}) = (1 - \alpha)|F(\mathbf{h})|^2 + \alpha|F(\mathbf{m}_x\mathbf{h})|^2,$$

which may be re-expressed as

$$Y(\mathbf{h}) = |F_1(\mathbf{h})|^2 + |F_2(\mathbf{h})|^2 + (1 - 2\alpha)[F_1(\mathbf{h})F_2(\mathbf{h})^* + F_1(\mathbf{h})^*F_2(\mathbf{h})],$$

where $F_1(\mathbf{h}) = [F(\mathbf{h}) + (-1)^{m_M}F(\mathbf{m}_x\mathbf{h})]/2$ and $F_2(\mathbf{H}) = [F(\mathbf{h}) - (-1)^{m_M}F(\mathbf{m}_x\mathbf{h})]/2$. Choosing $\mathbf{d}_M = 0$ as the origin, $F(\mathbf{m}_x\mathbf{h}) = (-1)^{m_M}F(\mathbf{h})$ for the incommensurate case due to the symmetry operator $\{\mathbf{m}_x|0, 0, 0, \frac{1}{2}\}$, so that $F_2(\mathbf{h}) = 0$ and $Y(\mathbf{h}) = Y(\mathbf{m}_x\mathbf{h}) = |F(\mathbf{h})|^2$. For the crystal studied, however, small but significant intensity differences between reflections $\mathbf{h}$ and $\mathbf{m}_x\mathbf{h}$ were observed, particularly for data of index 5 and 6. The refinement of $Ta_{22}W_4O_{67}$ thus included a twin ratio parameter which refined to $\sim 0.9 : 0.1$. The *mmm* diffraction symmetry of the $Ta_{74}W_6O_{203}$ data meant that no such twin ratio parameter was required in that case.

The initial structure model for $Ta_{22}W_4O_{67}$ was obtained using comparative refinement of the most extensively collected $\lambda = 1.2741$ Å data set (note that this data set does not greatly distinguish between Ta and W). The parent substructure positions and occupancies were assumed to be as given above (see §2). All displacive modulation wave amplitudes were then set to zero, except for the three dominant metal-atom modulation wave amplitudes $a_{Mx}(\mathbf{q}_M)$, $a_{Mx}(3\mathbf{q}_M)$ and $a_{My}(2\mathbf{q}_M)$. Eight sign combinations were tested in a five-parameter refinement of scale, overall isotropic temperature parameter and magnitude of these three modulation wave amplitudes. A least-squares refinement, starting with magnitudes for these parameters of 0.1 Å, showed that two equivalent sign combinations were far superior to the others. These two equivalent sign combinations corresponded to an orientation option of the same structure for $Ta_{22}W_4O_{67}$ and to an origin choice for $Ta_{74}W_6O_{203}$. Having determined the correct sign combination, the corresponding modulation wave amplitudes, $a_{Mx}(\mathbf{q}_M)$, $a_{Mx}(3\mathbf{q}_M)$ and $a_{My}(2\mathbf{q}_M)$, refined to essentially the values given in Table 1 under the column headed 'ordered model'. Subsequent density maps then allowed the location of all O-atom sites.

Having determined $a_{Mx}(\mathbf{q}_M)$, $a_{Mx}(3\mathbf{q}_M)$ and $a_{My}(2\mathbf{q}_M)$, all other displacive modulation wave amplitudes could then be refined from zero, although refinement of the large-magnitude O-substructure modulation wave amplitudes $\{a_{3x}([2m_O + 1]\mathbf{q}_O)$, $2m_O + 1 = 1, 3, 5$; and $a_{3y}(2\mathbf{q}_O)\}$ was the next sensible step in a hierarchical refinement. The sign options on these major O substructure modulation waves were also checked by comparative refinement and found to be as given in Table 1 under the column headed 'ordered model'.

The initial $Ta_{74}W_6O_{203}$ model used the parameters from $Ta_{22}W_4O_{67}$. Note that if the relative origins of the two substructures were not locked in, the commensurate *Pbam* and *Pbmm* models should fit the data equally well (Pérez-Mato, 1991). This, however, was not the case. Comparison of refinements in space groups *Pbam* and *Pbmm* showed that the structure always refined better in *Pbam* than *Pbmm*, see, for example, models 1 and *Pbmm* of Table 5.

The similarity of the major displacive modulation wave amplitudes for the two structures was thus

clearly established. Thus in Table 1, the parameters $a_{\mu x}([2m_M + 1]\mathbf{q}_M)$, $\mu = 1, 2$; $2m_M + 1 = 1, 3$; $a_{\mu y}(2\mathbf{q}_M)$, $\mu = 1, 2$; $a_{3x}([2m_O + 1]\mathbf{q}_O)$, $2m_O + 1 = 1, 3, 5$; $a_{3y}(2\mathbf{q}_O)$ for each of the structures are most significant and quite reliable. These fundamental parameters are essentially independent of the value of $\mathbf{d}_O - \mathbf{d}_M$, *i.e.* of whether or not the structures are indeed commensurate. The magnitudes of all other displacive modulation wave amplitudes refined to very small values $<\sim 0.02$ Å.

Having successfully refined the major displacive amplitudes, the next consideration was the W atom and O vacancy distribution. To this end, data sets at other wavelengths closer to the Ta L_{III} absorption edge were also collected. Using the 1.2563 Å data set, it was found possible to refine Ta/W ordering for $Ta_{74}W_6O_{203}$ from any starting point. In the case of $Ta_{22}W_4O_{67}$, it was found necessary to first exclude some few weak reflections with $|F_{calc}| < 0.4|F_{obs}|$ to eliminate false minima. Only *ca* 1% of reflections were excluded by this process and better refinement statistics were then obtained for the remaining data. It was then possible to refine Ta/W ordering from any starting point. The significant improvement in refinement statistics upon Ta/W ordering is clear from a comparison of models 1 and 2 in Table 5. The refined occupancies for these ordered models both in terms of occupational modulation wave amplitudes and individual atom-based occupancies are listed in Table 6. These refinements suggest that W atoms tend to occupy sites over a limited range of $\omega(\mathbf{t}_M)$ in each case, corresponding essentially to sites *M*1 and *M*7 of the $Ta_{22}W_4O_{67}$ structure and *M*1 of the $Ta_{74}W_6O_{203}$ structure.

Atoms were refined with individual anisotropic thermal parameters, U_{ij}. The only truly notable deviation away from mean values was in the U_{zz} values of the metal atoms. *M*1 and *M*7 of the $Ta_{22}W_4O_{67}$ structure and *M*1 of the $Ta_{74}W_6O_{203}$ structure had rather higher U_{zz} values than all other metal atoms, *i.e.* the sites with excess U_{zz} thermal motion are also the W-bearing sites. This excess U_{zz} thermal motion is taken as indicative that the same range of $\omega(\mathbf{t}_M)$ is also associated with oxygen vacancies on the O_M ($\mu = 2$) site. The standard deviations for these latter oxygen site occupancies, however, were found to be too large to allow them to be meaningfully refined and so they were given model imposed values, *i.e.* O substructure oxygen vacancies were constrained to be associated with Ta on W-bearing metal-atom sites (in the ratio of one vacancy per two Ta atoms).

Determination of the small magnitude, displacive modulation wave amplitudes for $m_M > 3$ and $m_O > 5$ was carried out after the introduction of disorder.

5.1. *A faulted or disordered model*

While the refinement statistics for the above fully ordered models were already quite satisfactory [see the refinement statistics for the ordered models (model 2) given in Table 5], the quality of refinement appeared to deteriorate as m_M increased, suggesting that data fitting might be improved by incorporation of some sort of fluctuation in the relative origin of the two substructures, *i.e.* in δ. What the nature of this disorder might be is suggested by the resultant $C112/m$ space-group symmetry of $Ta_{22}W_4O_{67}$.

As mentioned above, $C112/m$ space-group symmetry for $Ta_{22}W_4O_{67}$ implies a 'lock-in' of δ to $(2N + 1)/52$, with N an integer. Similarly, *Pbam* space-group symmetry for $Ta_{74}W_6O_{203}$ implies a 'lock-in' of δ to $(2N + 1)/32$, with N an integer. In each case, changing N by the smallest possible amount, *i.e.* by ± 1, corresponds to a discrete jump in the relative origin of the two substructures by $\pm\frac{1}{26}\mathbf{b}_O$ and $\pm\frac{1}{16}\mathbf{b}_O$, respectively. The effect of such phase slips is to reflect the original structures through mirror planes, shown as dashed lines in Figs. 3 and 4. These mirror planes perpendicular to **b** pass approximately through atoms *M*4 in Figs. 3 and 4, the exact position being a refinable parameter. The overall $C112/m$ and *Pbam* space-group symmetries are maintained provided the volume fraction of the $N' = N + 1$ and $N' = N - 1$ portions of the structure are equal.

It was considered that the improvement in refinement statistics associated with such disorder models, while not dramatic, was significant (*cf.* models 2 and 3 of Table 5). Model 3, for $Ta_{22}W_4O_{67}$, gave slightly negative values for the W occupancy of sites *M*3, *M*4 and *M*5. In model 4, these values are constrained to zero and the remaining site occupancies refined. There is a negligible difference in refinement statistics. The final displacive modulation wave amplitudes listed in Table 1 were obtained using Model 4 for $Ta_{22}W_4O_{67}$ and Model 3 for $Ta_{74}W_6O_{203}$. These models are now discussed for each of the compositions.

5.2. *Refinement of the C112/m structure*

Refinement using the $\lambda = 1.2563$ Å data most clearly distinguished between W and Ta. In the non-disordered model (see model 2 of Tables 5 and 6), significant W occupancy occurs on the *M*2 and *M*6 sites in addition to the larger occupancies on *M*1 and *M*7. Effectively the same occupancy distribution can also be obtained using the above disorder model in which the W:Ta ratio is constrained to be 0:1 for sites *M*3, *M*4 and *M*5 and refineable parameters elsewhere (model 4 of Tables 5 and 6). The resultant W:Ta distribution satisfies stoichiometry, is suggested by the refined occupancies of model 2 and avoids unnecessary occupational degrees of freedom. The more extensive 1.2741 Å data set was used to refine all parameters, except the Ta/W ordering which was refined using the 1.2563 Å data. The final refinement for each wavelength was started with the same parameters and gave values which agreed to within 3σ.

Table 1. *Final modulation wave parameters* (Å)

	$Ta_{22}W_4O_{67}$	$Ta_{74}W_6O_{203}$	$Ta_{22}W_4O_{67}$
$\mathbf{d}_O$	$\frac{1}{4}\mathbf{a}_O + \frac{21}{4}\mathbf{b}_O$	$\frac{13}{2}\mathbf{b}_O$	Ordered model
$\mathbf{d}_M$	0	$\frac{3}{4}\mathbf{a}_M + \frac{3}{4}\mathbf{b}_M$	
M substructure parameters ($\mu = 1$ for *M*, $\mu = 2$ for O_M)			
$\mathbf{b}_O^*.(\mathbf{d}_M - \mathbf{d}_O)$, modulo 1	$-\frac{1}{4}$	$-\frac{1}{4} - \frac{1}{32}$	
Wavelength (Å)	1.2741	1.2563	1.2741
$a_{1x}(1\mathbf{q}_M)$	0.2082 (5)	0.2220 (3)	0.2112 (5)
$a_{1x}(3\mathbf{q}_M)$	0.2690 (5)	0.2843 (5)	0.2520 (5)
$a_{1x}(5\mathbf{q}_M)$	−0.0006 (4)	−0.0011 (3)	−0.0001 (4)
$a_{1x}(7\mathbf{q}_M)$	0.0182 (5)	0.0183 (3)	0.0125 (5)
$a_{1x}(9\mathbf{q}_M)$	−0.0021 (6)		−0.0019 (6)
$a_{1x}(11\mathbf{q}_M)$	0.0*		0.0*
$a_{1y}(2\mathbf{q}_M)$	−0.1232 (4)	−0.1345 (4)	−0.1221 (4)
$a_{1y}(4\mathbf{q}_M)$	−0.0084 (3)	−0.0062 (3)	−0.0075 (3)
$a_{1y}(6\mathbf{q}_M)$	0.0092 (3)	0.0098 (3)	0.0071 (3)
$a_{1y}(8\mathbf{q}_M)$	−0.0068 (3)	−0.0106 (3)	−0.0045 (3)
$a_{1y}(10\mathbf{q}_M)$ *etc.*	0.0*		0.0*
$a_{2x}(1\mathbf{q}_M)$	0.342 (6)	0.321 (4)	0.348 (7)
$a_{2x}(3\mathbf{q}_M)$	0.185 (6)	0.198 (4)	0.171 (6)
$a_{2x}(5\mathbf{q}_M)$	−0.013 (6)	0.005 (4)	−0.012 (6)
$a_{2x}(7\mathbf{q}_M)$	0.000 (6)	−0.008 (4)	−0.001 (5)
$a_{2x}(9\mathbf{q}_M)$	−0.016 (8)		−0.010 (7)
$a_{2x}(11\mathbf{q}_M)$	0.0*		0.0*
$a_{2y}(2\mathbf{q}_M)$	−0.261 (6)	−0.242 (4)	−0.249 (6)
$a_{2y}(4\mathbf{q}_M)$	−0.002 (5)	0.038 (4)	0.000 (5)
$a_{2y}(6\mathbf{q}_M)$	0.007 (5)	−0.023 (4)	0.010 (5)
$a_{2y}(8\mathbf{q}_M)$	−0.014 (5)	0.007 (3)	−0.010 (5)
$a_{2y}(10\mathbf{q}_M)$ *etc.*	0.0*		0.0*
O substructure parameters ($\mu = 3$)			
$\mathbf{b}_M^*.(\mathbf{d}_O - \mathbf{d}_M)$, modulo 1	$\frac{1}{4}$	$\frac{1}{4}$	Ordered model
$a_{3x}(1\mathbf{q}_M)$	0.776 (5)	0.782 (3)	0.776 (5)
$a_{3x}(3\mathbf{q}_M)$	0.081 (4)	0.090 (3)	0.085 (4)
$a_{3x}(5\mathbf{q}_M)$	0.246 (4)	0.273 (3)	0.226 (4)
$a_{3x}(7\mathbf{q}_M)$	−0.009 (4)	−0.015 (3)	−0.005 (4)
$a_{3x}(9\mathbf{q}_M)$	−0.016 (4)	−0.013 (3)	−0.016 (4)
$a_{3x}(11\mathbf{q}_M)$	0.010 (5)	0.012 (4)	0.011 (5)
$a_{3x}(13\mathbf{q}_M)$	−0.011 (6)		−0.003 (6)
$a_{3x}(15\mathbf{q}_M)$	0.010 (7)		0.002 (7)
$a_{3x}(17\mathbf{q}_M)$ *etc.*	0.0*		0.0*
$a_{3y}(2\mathbf{q}_M)$	−0.310 (4)	−0.320 (3)	−0.307 (4)
$a_{3y}(4\mathbf{q}_M)$	−0.016 (4)	−0.017 (3)	−0.015 (4)
$a_{3y}(6\mathbf{q}_M)$	0.012 (4)	0.009 (3)	0.014 (4)
$a_{3y}(8\mathbf{q}_M)$	0.000 (4)	0.002 (3)	0.000 (4)
$a_{3y}(10\mathbf{q}_M)$	0.015 (4)	0.008 (3)	0.011 (4)
$a_{3y}(12\mathbf{q}_M)$	−0.007 (4)	−0.004 (3)	−0.002 (4)
$a_{3y}(14\mathbf{q}_M)$ *etc.*	0.0*		0.0*

* Values set to zero.

In the final disorder model (model 4), the major fraction, 0.686, of the structure was found to be as shown in Fig. 3, and 0.157 (10) in each of two orientations associated with disorder across the planes shown as dashed lines in Fig. 3. These latter fractions are equal because overall $C112/m$ symmetry was maintained. The location of the disorder planes refined to $\pm 4.493\mathbf{b}_M = \pm 7.257\mathbf{b}_O$ (see Fig. 3) with an error of 0.002 Å. The final refined twin ratio was 0.906:0.094 (4).

The final displacive modulation wave amplitudes are listed in Table 1. Not all the displacive modulation wave amplitudes were refined. The fixed, highest order m_M, modulation wave amplitudes are marked *. It was found by monitoring apparent valences (see Part I) as an indication of correctness that it was not possible to obtain meaningful refinement for these parameters, and better results were obtained by fixing their values at 0.0. The higher apparent valences of the three-coordinate O atoms had been up to 0.1 greater when these parameters were included in the refinement. The final occupancy parameters are listed in Table 6 while the final values for the non-zero average substructure thermal parameters and the U_{zz}'s of the metal atoms are listed in Table 3. The refinement statistics, and the number of reflections to which they apply are given in Table 2.

Table 2. *Final refinement statistics for* $Ta_{22}W_4O_{67}$ *and* $Ta_{74}W_6O_{203}$

Data set 1/2/3	10^4R_1	10^4wR	G.o.f.
$Ta_{22}W_4O_{67}$			
238/71/80 $m_M = 0$ data	495/249/273	829/322/335	1.83/0.86/0.87
458/116/134 $m_M = 1$ data	451/389/465	803/615/569	1.84/1.58/1.46
484/141/156 $m_M = 2$ data	495/280/386	936/585/681	2.16/1.48/1.72
484/114/133 $m_M = 3$ data	485/250/275	842/456/764	1.94/1.19/1.95
477/132/159 $m_M = 4$ data	467/385/472	860/637/880	1.98/1.36/1.94
476/106/122 $m_M = 5$ data	480/448/500	887/624/719	1.98/1.26/1.44
465/98/125 $m_M = 6$ data	498/387/580	856/542/823	1.90/1.07/1.54
288/168/167 $I < 3\sigma(I)$ data			3.46/1.41/1.75
All 3082/778/909 used data	481/299/354	863/554/702	1.96/1.31/1.64
$Ta_{74}W_6O_{203}$			
164/487/144 $m_M = 0$ data	335/334/382	509/516/511	1.50/1.49/2.26
237/812/240 $m_M = 1$ data	763/792/876	1053/1082/1179	2.84/2.75/5.19
263/897/261 $m_M = 2$ data	514/548/685	820/889/1077	2.34/2.42/4.65
261/862/256 $m_M = 3$ data	426/471/475	669/711/696	1.94/1.95/3.10
238/816/222 $m_M = 4$ data	773/719/758	1115/1014/949	2.61/2.30/2.94
234/725/194 $m_M = 5$ data	749/720/1027	1114/1053/1152	2.45/2.33/3.20
210/641/183 $m_M = 6$ data	765/750/754	1018/1032/1001	2.20/2.20/2.91
99/338/89 $m_M = 7$ data	1337/1311/1510	1703/1567/1849	2.20/2.08/2.04
43/97/44 $m_M = 8$ data	2210/1944/1767	2371/2147/2254	2.42/2.37/2.45
394/1594/432 $I < 3\sigma(I)$ data			2.20/1.56/2.31
All 1748/5675/1632 used data	554/571/610	921/928/962	2.32/2.27/3.59

Numbers are sequential for data sets with $\lambda = 1.2741/1.2563/1.2571$.

$R_1 = \sum_{\mathbf{h}} ||F_{obs}(\mathbf{h})| - |F_{calc}(\mathbf{h})|| / \sum_{\mathbf{h}} |F_{obs}(\mathbf{h})|$.

$wR = [\sum_{\mathbf{h}} w_{\mathbf{h}}(|F_{obs}(\mathbf{h})| - |F_{calc}(\mathbf{h})|)^2 / \sum_{\mathbf{h}} w_{\mathbf{h}}|F_{obs}(\mathbf{h})|^2]^{1/2}$.

G.o.f. $= [\sum_{\mathbf{h}} w_{\mathbf{h}}(|F_{obs}(\mathbf{h})| - |F_{calc}(\mathbf{h})|)^2/(n-m)]^{1/2}$.

Table 3. *Final values for the non-zero average substructure thermal parameters and the* U_{zz}*'s of the metal atoms*

Non-zero average values of U_{ij} (10^{-3} Å^2)

	$Ta_{22}W_4O_{67}$			$Ta_{74}W_6O_{203}$		
	U_{xx}	U_{yy}	U_{zz}	U_{xx}	U_{yy}	U_{zz}
M-substructure						
M	10	5	21	8	12	27
O_M	6	17	20	10	18	0
O substructure						
O_O	10	9	10	6	15	14

Values of U_{zz} (10^{-3} Å^2) for the *M* sites

Structure	*M*1	*M*2	*M*3	*M*4	*M*5	*M*6	*M*7
$Ta_{22}W_4O_{67}$	64	18	7	4	5	5	61
$Ta_{74}W_6O_{203}$	48	22	20	18			

Errors are < 0.001 Å^2 for individual *M* atoms and *ca* 0.003 Å^2 for individual O atoms.

5.3. *Refinement of the Pbam structure*

In the case of $Ta_{74}W_6O_{203}$, the non-disordered model refinement (model 2) showed that nearly all the W was located on the $M1$ site with a quite minor amount on the $M2$ site. Effectively the same occupancy distribution can be obtained using a disorder model in which the W:Ta ratio is constrained to be 0.3:0.7 on the $M1$ site and 0:1 elsewhere (see model 3 in Table 5). The more extensive 1.2563 Å data set was used to refine all parameters. Starting with these parameters, refinement for the other wavelengths gave parameters that agreed to within 3σ.

The predominant fraction, 0.928, of the structure was found to be as shown in Fig. 4, with 0.036 (4) in each of two orientations associated with disorder across the planes shown as dashed lines in Fig. 4. These disorder planes were located at $\pm 1.236\mathbf{b}_M = \pm 2.009\mathbf{b}_O$. The final displacive modulation wave amplitudes are given in Table 1, the final occupancy parameters in Table 6 and the final thermal parameters in Table 3. The refinement statistics and the number of reflections to which they apply are given in Table 2.

6. Discussion of the structures

When described in terms of modulation wave amplitudes, the remarkable similarity of the two structures is immediately apparent (see Tables 1 and 6), despite the significant difference in composition and in wavevector magnitude. In the case of the displacive degrees of freedom, a limited number of low harmonic-order modulation wave amplitudes dominate the structure description as well as the diffraction pattern. There is up to 10% difference between equivalent (*i.e.* same harmonic order) modulation wave amplitudes. The extraordinary similarity between the two refined structures is best illustrated in the plots of various AMF's (described below) shown in Figs. 5–10. It is reasonable to expect that these parameters change little across the entire solid solution range, given the similarity between the W-rich end member and a mid-range composition. Projections of the structures down **c** are shown in Figs. 3 and 4. Atoms O_M, at $z = \pm\frac{1}{2}$, immediately above and below the metal atoms are not shown. Tables of atom-based parameters for $Ta_{22}W_4O_{67}$ and $Ta_{74}W_6O_{203}$ are presented in Part I.

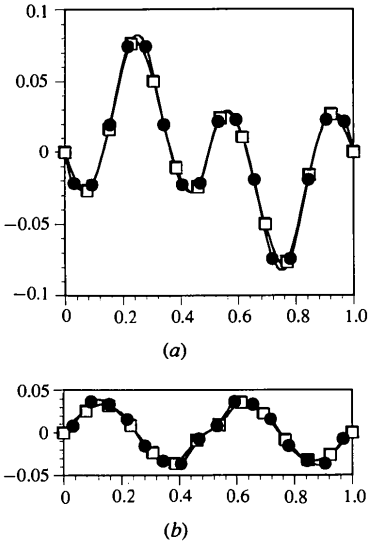

Fig. 5. The (*a*) *x* and (*b*) *y* displacements of the *M* atoms in fractional coordinates of the parent substructure axes a_M and b_M plotted as a function of $[\omega(\mathbf{t}_M) + \frac{1}{4}]$. Unfilled squares correspond to $Ta_{22}W_4O_{67}$; filled circles correspond to $Ta_{74}O_6W_{203}$. Expressed in these terms, the two structures are effectively identical. For convenience the vertical scales of the AMF's in Figs. 5 and 6 have been chosen to allow direct comparison of atomic displacements in Å.

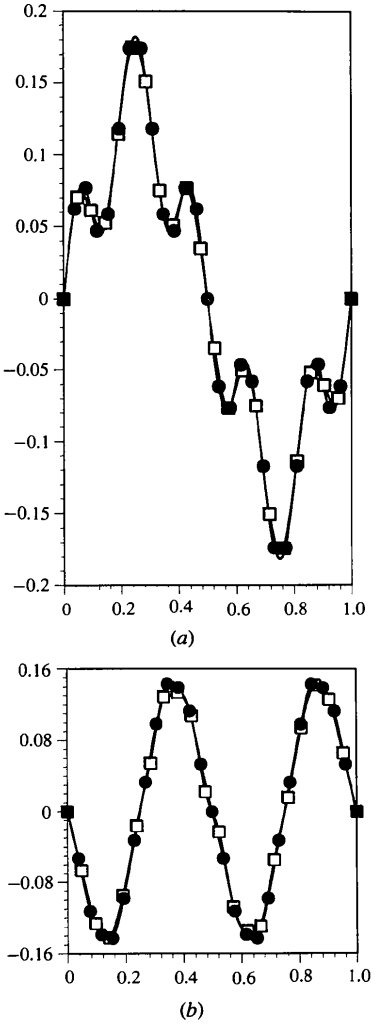

Fig. 6. The (*a*) *x* and (*b*) *y* displacements of the O atoms in fractional coordinates of the parent substructure axes a_O and b_O plotted as a function of $[-\omega(\mathbf{t}_O) - \frac{1}{4}]$. Unfilled squares correspond to $Ta_{22}W_4O_{67}$; filled circles correspond to $Ta_{74}O_6W_{203}$. As for the metal atoms, the AMF's for the two structures with quite different compositions superimpose.

6.1. *Evolution of the structure as a function of* $\omega(\mathbf{t}_M)$ *and* $\omega(\mathbf{t}_O)$

Atoms were labelled in Part I starting from the origins of the substructures as listed in Table 1 and incrementing according to the parent substructure translations $\mathbf{t}_M = \frac{1}{2}\mathbf{a}_M + \frac{3}{2}\mathbf{b}_M$ and $\mathbf{t}_O = \frac{1}{2}\mathbf{a}_O + \frac{5}{2}\mathbf{b}_O$ so that $\mathbf{q}_M.\mathbf{t}_M$, modulo 1, is $-\frac{1}{13}$ for $Ta_{22}W_4O_{67}$ and $-\frac{1}{16}$ for $Ta_{74}W_6O_{203}$ and $\mathbf{q}_O.\mathbf{t}_O$, modulo 1, is $\frac{1}{21}$ for $Ta_{22}W_4O_{67}$ and $\frac{1}{26}$ for $Ta_{74}W_6O_{203}$. Because the structures are commensurate, these are the smallest possible increments in the quantities $\omega(\mathbf{t}_M)$ and $\omega(\mathbf{t}_O)$, respectively. As discussed in Part I, when looking at the actual structure evolving along **b** it is useful to look at metal and in-plane oxygen coordination. Starting with the distorted octahedral site $M1$ (see Figs. 3 and 4), one can observe the evolution of the metal coordination as a function of $\omega(\mathbf{t}_M)$. A similar evolution occurs for the in-plane O atoms as a function of $\omega(\mathbf{t}_O)$. A different number of incremental steps are taken in the two cases to return to the same coordination environment. For an incommensurate structure $\omega(\mathbf{t}_M)$ or $\omega(\mathbf{t}_O)$ do not repeat the same values, modulo 1.

Figs. 5 and 6 show the x and y displacements in fractional coordinates relative to the relevant parent substructure unit cell for the metal atoms of the M substructure as a function of $\omega(\mathbf{t}_M) + \frac{1}{4}$, modulo an integer, and for the O atoms of the O substructure as a function of $-\omega(\mathbf{t}_O) - \frac{1}{4}$, modulo an integer. The curves for the two structures studied are shown superimposed, with points corresponding to atom parent positions in space groups $C112m$ and $Pbam$ indicated. An M atom on a centre of inversion corresponds to $\omega(\mathbf{t}_M) = \pm\frac{1}{4}$ and an O atom on a centre of inversion corresponds to $\omega(\mathbf{t}_O) = \pm\frac{1}{4}$.

The M parent substructure approximates a primitive hexagonal array (see Table 4) since $a_M/b_M \sim 3^{1/2}/2$.

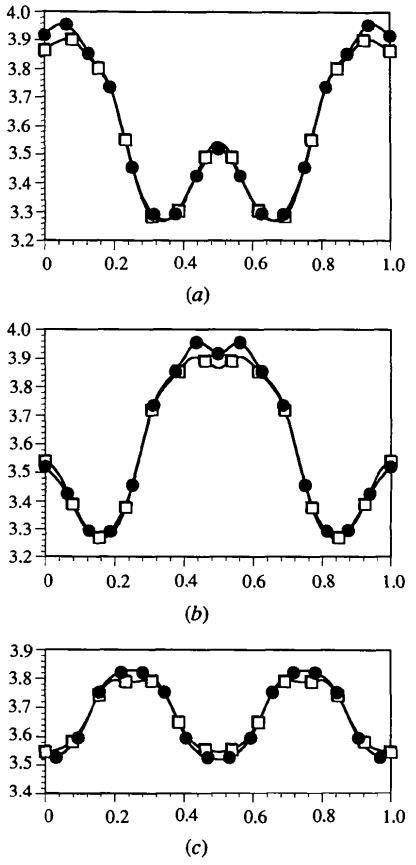

Fig. 7. M—M distances, in Å plotted as a function of $[\omega(\mathbf{t}_M) + \frac{1}{4} + \mathbf{b}_O^*.\mathbf{r}_M]$, where $2\mathbf{r}_M = [(a)\ (\mathbf{a}_M + \mathbf{b}_M)/2,\ (b)\ (\mathbf{a}_M - \mathbf{b}_M)/2,\ (c)\ \mathbf{b}_M]$ is the M—M separation distance in the parent substructure. Unfilled squares correspond to $Ta_{22}W_4O_{67}$; filled circles correspond to $Ta_{74}O_6W_{203}$.

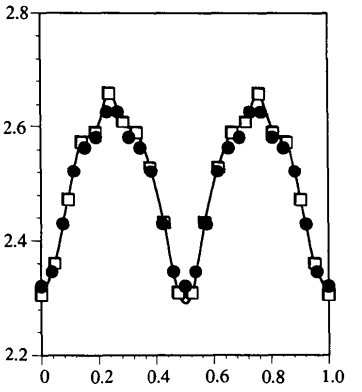

Fig. 8. O—O distances along b_O, in Å, plotted as a function of $[-\omega(\mathbf{t}_O) - \frac{1}{4} - \mathbf{b}_M^*.\frac{1}{2}\mathbf{b}_O]$. Unfilled squares correspond to $Ta_{22}W_4O_{67}$; filled circles correspond to $Ta_{74}O_6W_{203}$.

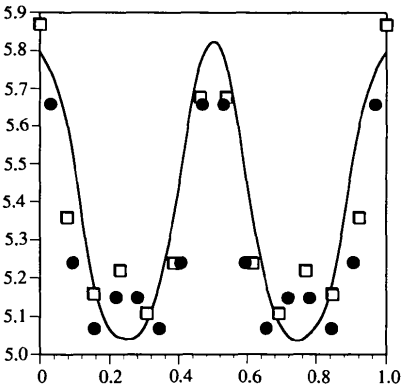

Fig. 9. The apparent valence of a Ta atom at $x, y, 0$ with an O atom at both $x, y, \frac{1}{2}$ and $x, y, -\frac{1}{2}$, plotted as a function of $[\omega(\mathbf{t}_M) + \frac{1}{4}]$. The continuous curve corresponds to the modulation parameters of the $Ta_{22}W_4O_{67}$ structure with those parameters which are less than 0.02 Å in magnitude set to zero. It is seen that these small terms create a bigger contrast between the AV = 6 and AV = 5 sites. Unfilled squares correspond to $Ta_{22}W_4O_{67}$; filled circles correspond to $Ta_{74}O_6W_{203}$.

Fig. 7 shows M—M distances plotted as a function of $[\omega(\mathbf{t}_M) + \frac{1}{4} + \mathbf{b}_O^*.\mathbf{r}_M]$, where $2\mathbf{r}_M$ is a vector corresponding to the relevant M—M separation distance in the parent substructure. These contacts vary by ±10% relative to their ideal close-packed separation of ~ 3.6 Å. In the parent O substructure, the O—O distance along $b_O \approx 2.25$ Å is much shorter than the ≈ 3.28 Å value in the other two directions, *i.e.* $(\mathbf{a}_O \pm \mathbf{b}_O)/2$. Fig. 8 shows O—O distances along $\mathbf{b}_O$ plotted as a function of $[-\omega(\mathbf{t}_O) - \frac{1}{4} - \mathbf{b}_M^*.\frac{1}{2}\mathbf{b}_O]$. The effect of the AMF's is to cause the minimum value to be *ca* 0.1 Å larger than b_O and the maximum *ca* 0.4 Å larger.

Fig. 9 shows the apparent valences of the M atom (see Part I), assuming no apical oxygen vacancies, as a function of $\omega(\mathbf{t}_M) + \frac{1}{4}$. The curve excludes all small modulation wave amplitudes (with magnitude less than 0.02 Å), whereas the plotted points include all parameters. The variation in AV is dominated by an $m_M = 2$ term. In isolation this term would make the AV decrease smoothly from a maximum, corresponding to an M atom on an inversion centre, to a minimum, corresponding to an M atom on a mirror plane. Higher-order terms make this plot more square-wave-like. Given that Ta has a formal valence of +5 and W of +6, it is evident that the effect of the small modulation wave amplitudes is to partition the chemical environments into AV = 5 and AV = 6 sites. Fig. 10 shows M—O distances as a function of $\omega(\mathbf{t}_M)$.

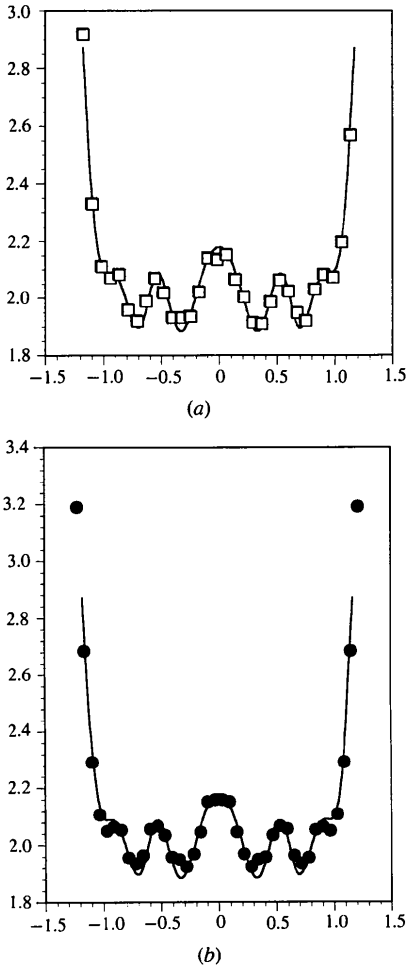

Fig. 10. A plot of M—O distances as a function of $\omega(\mathbf{t}_M)$. Each increment corresponds to a pseudo-translation of the metal atom by $(\mathbf{a}_M + 3\mathbf{b}_M)/2$ and a pseudo-translation of the O atom by $(\mathbf{a}_O + 5\mathbf{b}_O)/2$. The continuous curve corresponds to the modulation parameters of the $Ta_{22}W_4O_{67}$ structure with those parameters that are less than 0.02 Å in magnitude set to zero. Unfilled squares correspond to (*a*) $Ta_{22}W_4O_{67}$; filled circles correspond to (*b*) $Ta_{74}O_6W_{203}$.

Table 4. *Parent stucture dimensions* (Å)

Compound	$a_M = a_O$	$c_M = c_O$	b_M	b_O	d_1*	d_2*
$Ta_{22}W_4O_{67}$	6.1485 (5)	3.8559 (3)	3.6631 (1)	2.2676 (1)	3.5784 (3)	3.2766 (3)
$Ta_{74}W_6O_{203}$	6.1664 (5)	3.8731 (2)	3.6590 (1)	2.2517 (1)	3.5851 (3)	3.2823 (3)

* $d_1 = (1/2)(a_M^2 + b_M^2)^{1/2}$, $d_2 = (1/2)(a_O^2 + b_O^2)^{1/2}$.

6.2. *Compositional and site implications*

In composite modulated structures, where two mutually incommensurable parent substructures move past each other, it follows that there is a continuous range of chemical environments between two extremes. In the case of $(1-x)Ta_2O_5.xWO_3$, $0 \le x \le 0.267$, the O substructure consists solely of O atoms displaced from the *mmm* sites of the *Cmmm* symmetry parent because of interaction with the metal atoms of the M substructure. The resultant metal chemical environments range from distorted octahedral (4+2)-sites, which have an apparent valence (AV) of *ca* 6, to regular pentagonal bipyramidal (5 + 2)-sites, which have an AV of *ca* 5. On the basis of calculated AVs of the two extremes, the regular pentagonal bipyramidal sites can only accommodate Ta atoms, whereas the distorted octahedral sites can accommodate either W or Ta atoms, the latter by introducing an oxygen vacancy in one of the adjacent apical oxygen sites to give 4 + 1 coordination (see Part I).

We can divide the formulae for the three commensurate members mentioned in Part I, namely $Ta_{22}W_4O_{67}$, $Ta_{74}W_6O_{203}$ and L-Ta_2O_5, into three parts if we use a classification of metal sites in which $f = m/(m+n)$ is the fraction of metal sites of type 1, which are distorted octahedral sites capable of accommodating a W atom, and $n/(m+n)$ is the fraction of metal sites of Type 2, which are regular or distorted pentagonal bipyramidal sites for which W occupancy is unfavourable. The general three-part description of the solid-solution is then given by $W_pTa_{m-p}O_{(m+p)/2}$:Ta_nO_n:$O_{(4m+3n)/2}$ where the first two parts describe the M substructure and the third part describes the O substructure. Along **b**, a repeat of $(4m+3n)/2$ O_O atoms is equivalent to a repeat of

Table 5. *Comparative refinement statistics for* $Ta_{22}W_4O_{67}$ *and* $Ta_{74}W_6O_{203}$

$Ta_{22}W_4O_{67}$

Values of 10^4R_1 for 778 data with $\lambda = 1.2563$ Å and $I(\mathbf{h}) > 3\sigma(I(\mathbf{h}))$

Value of m_M	0	1	2	3	4	5	6	Overall
Model 1	239	464	546	516	692	605	632	440
Model 2	241	392	288	270	468	471	529	316
Model 3	243	395	270	246	386	447	381	296
Model 4	249	400	280	250	385	448	387	299

Values of 10^4R_1 for 3082 data with $\lambda = 1.2741$ and $I(\mathbf{h}) > 3\sigma(I(\mathbf{h}))$

Value of m_M	0	1	2	3	4	5	6	Overall
Model 1	576	522	544	553	534	588	591	556
Model 4	495	451	495	485	467	480	498	481

Model 1: No W ordering, no pseudo-mirror disorder, no twinning.
Model 2: All M occupancy modulation wave parameters varied but no pseudo-mirror disorder or twinning.
Model 3: All M occupancy modulation wave parameters varied, pseudo-mirror disorder and twinning fixed at value from 1.2741 Å data.
Model 4: 4 W occupancy parameters for $M1$, $M7$, $M2$, $M6$, pseudo-mirror disorder and twinning fixed at value from 1.2741 Å data.

$Ta_{74}W_6O_{203}$

Values of 10^4R_1 for 5675 data with $\lambda = 1.2563$ Å and $I(\mathbf{h}) > 3\sigma(I(\mathbf{h}))$

m_M	0	1	2	3	4	5	6	7	8	Overall
Model 1	361	797	569	492	773	731	768	1382	2112	595
Model 2	354	805	543	484	723	719	757	1262	2204	580
Model 3	334	792	548	471	719	720	750	1311	1944	571
Pbmm	880	836	718	557	832	1040	1051	3129	4091	833

Model 3: 0.3 W occupancy on $M1$, pseudo-mirror disorder varied (Models 1 and 2 as above).
Pbmm: *Pbmm* model refined with W occupancy randomly distributed but no other disorder.

Table 6. *Tungsten occupancies obtained from the* $\lambda = 1.2563$ *Å refinements*

$Ta_{22}W_4O_{67}$ in $C112/m$

Site	$M1$	$M2$	$M3$	$M4$	$M5$	$M6$	$M7$
Model 1	0.154	0.154	0.154	0.154	0.154	0.154	0.154
Model 2	0.586	0.114	−0.004	−0.049	−0.011	0.097	0.561
Model 3*	0.630	0.103	−0.006	−0.044	−0.038	0.097	0.572
	0.612	0.176	0.005	−0.043	−0.034	0.082	0.507
Model 4*	0.583	0.087	0.000	0.000	0.000	0.076	0.546
	0.571	0.158	0.012	0.000	0.000	0.066	0.538

$Ta_{74}W_6O_{203}$ in $Pbam$

Site	$M1$	$M2$	$M3$	$M4$
Model 1	0.075	0.075	0.075	0.075
Model 2	0.315	0.008 (7)	−0.014 (7)	−0.009 (7)
Model 3*	0.300	0.000	0.000	0.000
	0.264	0.036 (4)	0.000	0.000

Occupancy modulation parameters $P_\mu(2m_M\mathbf{q}_M)$ for tungsten

$2m_M$	0	2	4	6	8	10	12
$Ta_{22}W_4O_{67}$							
Model 2	0.154	−0.284 (10)	0.134 (7)	−0.075 (10)	0.024 (10)	0.014 (25)	−0.070 (33)
Model 4	0.154	−0.256 (10)	0.153 (7)	−0.076 (10)	0.031 (10)	0.020 (25)	−0.067 (33)
$Ta_{74}W_6O_{203}$							
Model 3	0.075	−0.139	0.106	−0.057			

*Models 3 and 4 include disorder across pseudo-mirror planes. Each of the three components of the structure before disordering has the occupancy distribution listed in the first line. The average occupancies after disordering are listed in the second line. Standard deviations were calculated to be *ca* 0.02. Models are as for Table 5.
The values listed are for models (see Table 5) before pseudo-mirror plane disordering is applied.

$(m + n)$ M_M atoms, m on sites of type 1 and n on sites of type 2, *i.e.*

$$b_M/b_O = \tfrac{3}{2} + \tfrac{1}{2}f.$$

This result does not depend on the fraction of W atoms, but on the fraction of sites capable of accommodating W atoms, *i.e.* sites that require an O_M vacancy for each two Ta atoms on the adjacent M site.

If m and n are integers the structure will be commensurate. It is always possible to select a centrosymmetric three-dimensional space group for the resulting superstructures in which there is an organized distribution of M_M sites of Types 1 and 2. In none of the resulting space groups does a mirror plane perpendicular to **b** result, *i.e.* in our idealized description, the structures never manage to place two sites of type 1 next to each other, irrespective of the value of b_M/b_O. We identify the space group of highest symmetry as either $C112/m$ or $Pbam$. The lower-symmetry space groups $C11m$ and $Pb2_1m$ also allow this ordering, but $C2mm$ and $Pbmm$ do not.

References

JANNER, A. & JANSSEN, T. (1980). *Acta Cryst.* A**36**, 399–415.

PÉREZ-MATO, J. M. (1991). *Methods of Structural Analysis of Modulated Structures and Quasi-Crystals*, edited by J. M. PÉREZ-MATO, F. J. ZÚÑIGA & G. MADARIAGA, pp. 117–128. World Scientific, Singapore.

PÉREZ-MATO, J. M., MADARIAGA, G., ZÚÑIGA, F. J. & GARCIA ARRIBAS, A. (1987). *Acta Cryst.* A**43**, 216–226.

RAE, A. D. (1989). *RAELS89. A Comprehensive Constrained Least Squares Refinement Program.* Univ. of New South Wales, Australia.

RAE, A. D., THOMPSON, J. G., WITHERS, R. L. & WILLIS, A. C. (1991). *Acta Cryst.* B**46**, 474–487.

ROTH, R. S. & STEPHENSON, N. C. (1970). *Chemistry of Extended Defects in Non-Metallic Solids*, edited by L. EYRING & M. O'KEEFFE, pp. 167–182. North-Holland Publishing Company, Amsterdam.

ROTH, R. S., WARING, J. L. & PARKER, H. S. (1970). *J. Solid State Chem.* **2**, 445–461.

SCHMID, S., THOMPSON, J. G., RAE, A. D., BUTLER, B. D., WITHERS, R. L., ISHIZAWA, N. & KISHIMOTO, S. (1995). *Acta Cryst.* B**51**, 698–708.

SCHMID, S., WITHERS, R. L. & THOMPSON, J. G. (1992). *J. Solid State Chem.* **99**, 226–242.

SMAALEN, S. VAN (1991). *Phys. Rev. B*, **43**, 11330–11341.

WIEGERS, G. A., MEETSMA, A., HAANGE, R. J., VAN SMAALEN, S., DE BOER, J. L., MEERSCHAUT, A., RABU, P. & ROUXEL, J. (1990). *Acta Cryst.* B**46**, 324–332.

WILLIAMS, J. M., TILLEY, R. J. D., HARBURN, G. & WILLIAMS, R. P. (1991). *J. Solid State Chem.* **95**, 111–125.

WITHERS, R. L., SCHMID, S. & THOMPSON, J. G. (1993). *Acta Cryst.* B**49**, 941–951.

WOLFF, P. M. DE, JANSSEN, T. & JANNER, A. (1981). *Acta Cryst.* A**37**, 625–636.

YAMAMOTO, A. (1992). *Acta Cryst.* A**48**, 476–483.

YAMAMOTO, A. (1993). *Acta Cryst.* A**49**, 831–846.

YAMAMOTO, A. & NAKAZAWA, H. (1982). *Acta Cryst.* A**38**, 79–86.

Acta Cryst. (1995). B**51**, 721–733

Thermal Parameters for Minerals of the Olivine Group: their Implication on Vibrational Spectra, Thermodynamic Functions and Transferable Force Fields

BY TULLIO PILATI

Centro CNR per lo Studio delle Relazioni fra Struttura e Reattività Chimica, Via Golgi 19, *I*-20133 *Milano, Italy*

FRANCESCO DEMARTIN

Istituto di Chimica Strutturistica Inorganica, Università degli Studi, Via Venezian 21, *I*-20133 *Milano, Italy*

AND CARLO M. GRAMACCIOLI

Dipartimento di Scienze della Terra, Università degli Studi, e Centro CNR, Via Botticelli 23, *I*-20133 *Milano, Italy*

(*Received* 12 *May* 1994; *accepted* 12 *December* 1994)

Abstract

Atomic displacement parameters (a.d.p.'s) and vibrational entropies have been calculated for some minerals of the olivine group, such as forsterite (α-Mg_2SiO_4), fayalite (Fe_2SiO_4), tephroite (Mn_2SiO_4) and monticellite ($CaMgSiO_4$), for which accurate experimental data are available; the calculations were also extended to glaucochroite ($CaMnSiO_4$). For these purposes, a rigid-ion Born–von Karman model has been applied, using empirical atomic charges and force fields derived from a best fit to the Raman–IR spectra of all these minerals and to the experimental phonon dispersion curves of forsterite and quartz. The agreement between theoretical and experimental data is remarkably good, even at different temperatures, with the only exception of the displacement parameters of one O atom in monticellite, whose structure has been refined using a set of new data. The present model, whose successful extension to quartz proves a certain degree of transferability to other structural types, implies some reinterpretation of the IR–Raman vibrational spectra, especially for the low frequencies of tephroite and fayalite; agreement with the experimental (crystallographic) a.d.p.'s was essential for checking the validity of the empirical force fields. The values of vibrational entropy for fayalite and tephroite are consistent with complete magnetic disorder above 100 K; for fayalite the corrected Si—O bond lengths (average: 1.633 Å) are essentially temperature-independent under 1173 K.

Introduction

The calculation of a.d.p.'s for crystals can be particularly useful, as it provides the means to verify the physical meaning of the corresponding data obtained from structure refinement; moreover, on these grounds even the general validity of the model can be checked, as well as the force fields employed to interpret the vibrational behaviour of the crystals being studied.